JOURNAL OF COMPUTATIONAL PHYSICS 108, 314–326 (1993)

Coupling of Spectral Methods and the p-Version of the Finite Element Method for Elliptic Boundary Value Problems Containing Singularities*

W. CAI, H. C. LEE, AND H.-S. OH

Department of Mathematics, University of North Carolina at Charlotte, Charlotte, North Carolina 28223

Received September 30, 1991; revised August 5, 1992

In this paper, we study a coupling of spectral methods and the p-version finite element methods for elliptic boundary value problems containing singularities. The method of auxiliary mapping, which is a recent development to deal with domain singularities in the p-version of the finite element method, is employed to remove the pollution effect caused by singularities. An iterative interfacial coupling between spectral methods and the p-version of the finite element method is used and investigated numerically. The advantages of such an approach are demonstrated by the high accuracy of spectral methods for the smooth part of solutions and the flexibility of the p-version of the finite element method for dealing with singularities and irregular domains. The efficiency of the coupling method is also evaluated by comparing results obtained by this method with those obtained by the full finite element algorithm.

1. INTRODUCTION

Spectral methods have proved to be very effective for a variety of flow simulations. However, as global methods based on orthogonal polynomial approximations, they have some restrictions. The solutions of the physical problems should be smooth and the solution domain should be rectangular-like; otherwise spectral accuracy cannot be obtained.

To ease the restriction on the geometry, the spectral element method has been proposed. This method has been successfully applied to solve Navier–Stokes equations on domains which can be divided into rectangular-like subdomains [19, 22]. However, the spectral accuracy can only be achieved when the solution possesses no singularities. The singularities in the solutions can be divided roughly into two sources. First, there are singularities that come from "internal" aspects of the equations, as shock waves in conservation laws. Second, there are singularities that come from "external" aspects of the equations. These aspects include irregularities of domain, matching of different types of boundary conditions, nonsmoothness of data, and so on. For both cases, special attention has to be paid when spectral methods are applied. In this paper, we are concerned with problems containing the latter type of singularities. Spectral methods for shock waves have been studied in [9, 25].

In the spectral-element approach, the spectral approximation is applied on each of the subdomains. Therefore, for those subdomains where the solutions are not smooth, the high order accuracy of spectral methods will be destroyed, as usual. To eliminate as much as possible the influence of the irregularity of geometry on the overall accuracy of spectral methods, different approaches have to be adopted.

The finite element method is flexible in dealing with problems on irregular domains and with problems containing singularities. Moreover, the method of auxiliary mapping, developed recently [4, 20, 21], can handle such singularities effectively and economically when it is applied in the p-version of the finite element method. Thus, in this paper, we intend to couple spectral methods and the p-version of the finite element method. With this approach, we expect to keep the merits of the two approaches: the high accuracy of spectral methods for smooth solutions and the flexibility of the finite element method in dealing with irregular domain geometry. The essence of the coupling method is dividing a given domain Ω into large rectangular subdomains Ω_{sp} and the remaining part $\Omega_{fe} = \Omega \backslash \Omega_{sp}$, and then applying spectral methods on Ω_{sp} and the p-version of the finite element method on Ω_{fe}. Here the domain Ω is divided so that the subdomains Ω_{sp} do not contain any singularities. The coupling of spectral and the h-version finite element methods has been attempted in [8]; however, the essential problem of singularities in the solutions has not been addressed.

* This work was supported in part by NSF Grants ASC-9005874. Computing facility has been provided by a research grant from the North Carolina Supercomputer Center.

0021-9991/93 $5.00

Like any other hybrid method, the essential issue in coupling two types of numerical methods is a correct and efficient formulation of matching conditions on the interface where two different methods are patched. In [8], based on the variational argument of the original elliptic equations, several types of interface conditions have been suggested and studied. There the solutions from both the spectral and the finite element methods are coupled, resulting in large systems of algebraic equations to solve.

In [10], an iterative interface technique was suggested to match two spectral solutions along a common interface. With such a technique, solutions in the spectral domain and the finite element domain are determined separately and sequentially, and the solutions in separate domains are coupled through the boundary condition on the interfaces. The process of iteration stops when some prescribed criteria is satisfied.

An iterative interface coupling of spectral and finite difference methods for smooth solutions on arbitrary domains has been examined [17]. This approach for treating interfaces have also been used in [12–14] in coupling different types of numerical methods for numerical solutions of elliptic, parabolic, and hyperbolic partial differential equations. The novelty in our approach lies in coupling spectral and the p-version finite element methods; within the p-version of the finite element method, the method of auxiliary mapping is used.

With the device of an auxiliary mapping [4] in the framework of the p-version of the finite element method on singular regions Ω_{fe}, the pollution effect on spectral subdomains Ω_{sp} caused by singularities can be removed completely or can be reduced significantly.

As a first part of our investigation of this coupling method, we test the method on Helmholtz equations on polygonal domains which have re-entrant corners or cracks. The motivation to use Helmholtz equations as model problems is twofold. First, many problems in solid mechanics and electro-magnetics are related to the solution of these equations. Second, in the spectral simulations of Navier–Stokes equations [19], the diffusion term is often treated implicitly and the Helmholtz equation has to be solved in each time step. Thus, it is of practical interest to have an accurate solution of the Helmholtz equation. We can increase overall accuracy of spectral discretization of Navier–Stokes equations.

This paper is organized as follows. In Section 2, we introduce numerical techniques to be used in the coupling of spectral methods and the finite element method. In Section 3, numerical results for the Helmholtz equation on different irregular domains are presented. We also give a comparison in terms of accuracy and CPU time between results obtained by our coupling method and the results obtained by the p-version of the finite element method. Finally, concluding remarks are given in Section 4.

2. NUMERICAL METHODS

In this section, we introduce some numerical techniques that are used in coupling spectral methods with the finite element method. They are the method of auxiliary mapping [4, 20, 21] in the framework of the p-version of the finite element method, the pseudospectral Chebyshev collocation methods [10, 15] and the iterative interface method [11, 26].

Let us consider the following elliptic boundary value problem:

$$-\Delta u + \mu u = f \qquad \text{in } \Omega, \tag{1}$$

$$u = g \qquad \text{on } \Gamma_D, \tag{2}$$

$$\frac{\partial u}{\partial n} = h \qquad \text{on } \Gamma_N, \tag{3}$$

where $\bar{\Gamma}_D \cup \bar{\Gamma}_N = \partial\Omega$, Ω is a polygonal domain, $\mu \geqslant 0$, measure $(\Gamma_D) > 0$, $f \in L^2(\Omega)$, and $\partial u/\partial n$ is the outward normal derivative to Γ_N.

For regularity assumptions on g and h, we refer to Theorem 7.53 of [1] and Theorem 3.1 of [2].

2.1. The Method of Auxiliary Mapping in the Framework of the p-Version of the Finite Element Method

The results and arguments of this section are essentially unchanged if the Laplacian Δ is replaced by the general elliptic operator $\mathscr{L} = \sum_{i,j} \partial/\partial x_j (a_{ij} \partial/\partial x_i)$. Let G be a smooth extension of g with bounded support. Then by setting $w = u - G$, one can convert the elliptic problem (1)–(3) to the problem of the same type with homogeneous Dirichlet condition. Thus, it is sufficient to consider the problem (1)–(3) when $g = 0$.

Let $H^1(\Omega) = \{u \in L^2(\Omega) : Du \in L^2(\Omega)\}$ and $H^1_D(\Omega) = \{u \in H^1(\Omega) : u = 0 \text{ on } \Gamma_D\}$, where Du is the weak partial derivative, then the exact solution u_{ex} of (1)–(3) means the unique weak solution of the following problem: Find $u_{\text{ex}} \in H^1_D(\Omega)$ such that

$$B(u, v) = F(v) \qquad \text{for all} \quad v \in H^1_D(\Omega), \tag{4}$$

where

$$B(u, v) = \iint_\Omega \{\nabla u \cdot \nabla v + \mu(u \cdot v)\}\, d\Omega,$$

$$F(v) = \iint_\Omega fv\, d\Omega + \int_{\Gamma_N} hv\, d\gamma.$$

2.1.A. *The p-Version of the Finite Element Method*

There are three versions of the finite element method: the h-version, the p-version, and the h-p version. The h-version is the standard one, where the degree p of the elements is

fixed, usually at a low level, with $p=1$, 2, or 3 and the accuracy is achieved by properly refining the mesh. The p-version, in contrast, fixes the mesh and achieves better accuracy by increasing the degree p of the elements uniformly or selectively. The h-p version is a combination of both. The p-version of the finite element method is a new development [5, 7, 24]. Hence, in the following, we describe the p-version of the finite element method.

Let $S_p = \{w \in H_D^1(\Omega): w|_e \circ \Phi_e$ is a polynomial of degree p on E for every element $e\}$, where $\Phi_e: E \to e$ is the element mapping and E is the standard triangular element T or the standard rectangular element Q, according to whether e is a triangular element or a rectangular element. Then the p-version of the finite element method is defined as follows: Find $u_p \in S_p$ such that

$$B(u_p, v) = F(v) \qquad \text{for all} \quad v \in S_p. \tag{5}$$

The dimension of S_p will be called the degree of freedom and denoted by DOF. Let us note that in the p-version the triangulation of Ω is fixed and only the degree p of polynomial is increased. If $u_{ex} \in H_D^1(\Omega)$ is the exact solution then

$$\|u_p - u_{ex}\|_E = \min_{w \in S_p} \|w - u_{ex}\|_E,$$

where $\|\cdot\|_E$ is the energy norm.

Let $z = x_1 + ix_2$ and $\xi = \xi_1 + i\xi_2$. Let

$$S = \{(r, \theta): 0 \leqslant r \leqslant R,\ a \leqslant \theta \leqslant b\}, \tag{6}$$

$$S^* = \{(r^*, \theta^*): 0 \leqslant r^* \leqslant R^*,\ a^* \leqslant \theta^* \leqslant b^*\} \tag{7}$$

be two circular sectors on the z-plane and the ξ-plane, respectively. Suppose $\varphi^\alpha: S^* \to S$ is the conformal mapping defined by

$$z = \varphi^\alpha(\xi) = \xi^\alpha \tag{8}$$

and let ψ be the inverse function of φ^α; then the determinants of their Jacobians are

$$|J(\varphi^\alpha)| = \alpha^2 (r^*)^{2(\alpha-1)}, \qquad |J(\psi)| = \frac{1}{\alpha^2} r^{2(1-\alpha)/\alpha}, \tag{9}$$

respectively. Henceforth, the pull back of a function $f: S \to R$ by the conformal mapping φ^α is denoted by $\hat{f}$ (that is, $\hat{f} = f \circ \varphi^\alpha$).

The following was proved in [4, 21].

LEMMA 2.1. *For $u, v \in H^1(S)$, we have*

$$\iint_S \{\nabla u \cdot \nabla v + u \cdot v\}\, dx_1\, dx_2 = \iint_{S^*} \{\nabla \hat{u} \cdot \nabla \hat{v} + |J(\varphi^\alpha)|\, \hat{u} \cdot \hat{v}\}\, d\xi_1\, d\xi_2 \tag{10}$$

and

$$\iint_S f(x)\, v(x)\, dx = \iint_{S^*} \alpha^2 (\xi_1^2 + \xi_2^2)^{\alpha-1}\, \hat{f}(\xi)\, \hat{v}(\xi)\, d\xi, \tag{11}$$

2.1.B. *The Method of Auxiliary Mapping*

We now describe the *method of auxiliary mapping*, which can efficiently handle elliptic problems containing singularities (corner, jump of boundary data, interface of two or more materials). Suppose the exact solution u_{ex} has a corner singularity at P and suppose $f = 0$ on a neighborhood of P (argument is similar if $f \neq 0$ on any neighborhood of P). Let $\omega\pi$ be the interior angle at P. Then, on a neighborhood of P, the exact solution u_{ex} can be written as

$$u_{ex}(r, \theta) = \sum_{k=1}^{\infty} a_k r^{k/\omega} \sin(k\theta/\omega)$$

and the method goes as follows:

Step 1. Determination of the singular regions. At each singular point P, construct a sector S centered at P. Namely,

$$S = \{(r, \theta): 0 \leqslant r \leqslant R_0\} \cap \Omega,$$

where (r, θ) are the polar coordinates at P. Our method is not sensitive to the size of the radius R_0 since we are using the method in the p-version of the finite element method. However, when the singularity is very strong, it is better to choose for R_0 to be a little bit large if it is possible (i.e., $1 \geqslant R_0 \geqslant 0.5$).

Step 2. Selection of auxiliary mapping. Suppose $\omega > 1$. Then the auxiliary mapping can be chosen as follows: Let us define an auxiliary mapping by $\varphi^\omega: S^* \to S$, where $z = \varphi^\omega(\xi) = \xi^\omega$, a conformal mapping from the ξ-plane to the z-plane. Then the auxiliary mapping φ^ω transforms a singular function u_{ex} on S to an analytic function $\hat{u}_{ex}$ on S^*. That is,

$$\hat{u}_{ex}(r^*, \theta^*) = \sum_{k=1}^{\infty} a_k (r^*)^k \sin(k\theta^*).$$

Step 3. Triangulation of Ω. Generate a triangulation $\mathcal{T}_S$ on S as shown in Fig. 2.1. Then construct a triangulation $\mathcal{T}$ on Ω such that $\mathcal{T}|_S = \mathcal{T}_S$. Let $\mathcal{T}_S^*$ be the image of $\mathcal{T}_S$ under $(\varphi^\omega)^{-1}$ (see, Fig. 2.1).

For $e^* \in \mathcal{T}_S^*$ (and $e \in \mathcal{T}_0 = \mathcal{T} \setminus \mathcal{T}_S$), Φ_{e^*} (Φ_e) is the usual elemental mapping from the standard element E (which is either the reference triangle or rectangle according as e^* (e) is a triangular or a rectangular element) onto curvilinear elements e^* (e), respectively. Since we allow circular arcs as sides of elements, they could be of the *blending type* as

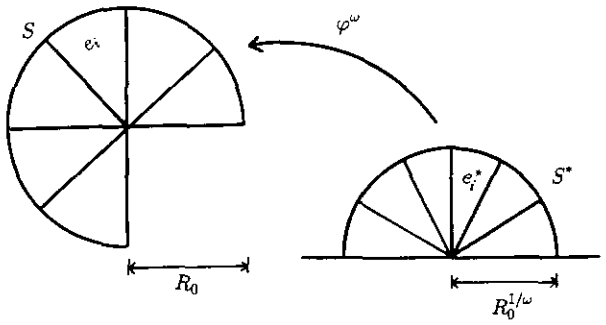

FIG. 2.1. *The schemes of an auxiliary mapping φ^ω, mesh on a circular sector S, and the corresponding mesh on S^*.*

those in Chapter 6 of [24] and satisfy the usual technical conditions [3] that lead to conforming elements.

Step 4. Computation of stiffness matrix and load vector. In computing local stiffness matrices and local load vectors,

- Use the standard elemental mapping Φ_e for the elements e in the nonsingular region $\Omega_0 = \Omega \backslash S$.
- Use the standard elemental mapping Φ_{e^*} for the elements e in the singular region S; in other words, local stiffness matrices and load vectors on the element e in the singular region are replaced by those computed on the elements $e_* = (\varphi^\omega)^{-1}(e)$ by using the right-hand sides of Eqs. (10) and (11).

Let Φ_e^S denote the special elemental mapping from E onto $e \in \mathscr{T}_q$ defined by $\Phi_e^S = \varphi^\omega \circ \Phi_{e^*}$. We will call this special elemental mapping Φ_e^S the *singular elemental mapping*. If Φ_e^S is used as the elemental mapping on the element e in a singular region S then the basis functions constructed through Φ_e^S will mimic the original singularity on S.

Let $\bar{\mathscr{N}}_i$ be the standard shape functions on E, $\mathscr{N}_i^* = \bar{\mathscr{N}}_i \circ \Phi_{e^*}^{-1}$ and $\mathscr{N}_i = \bar{\mathscr{N}}_i \circ (\Phi_e^S)^{-1}$. Then $\mathscr{N}_j \circ \varphi^\alpha = \mathscr{N}_j^*$. Hence, from Lemma 2.1, we have

$$\iint_e \{\nabla \mathscr{N}_i (\nabla \mathscr{N}_j)^{\mathrm{T}} + \mu (\mathscr{N}_i)(\mathscr{N}_j)^{\mathrm{T}}\}\, dx$$

$$= \iint_{e^*} \{\nabla \mathscr{N}_i^* (\nabla \mathscr{N}_j^*)^{\mathrm{T}} + \mu\, |J(\varphi^\alpha)|\, \mathscr{N}_i^* (\mathscr{N}_j^*)^{\mathrm{T}}\}\, d\xi \quad (12)$$

$$\iint_e f \mathscr{N}_j\, dx = \iint_{e^*} |\varphi^\alpha|\, \hat{f} \mathscr{N}_j^*\, d\xi. \quad (13)$$

Instead of computing the left-hand sides of (12)–(13) involving singular shape functions, we compute the right-hand sides of (12)–(13) for the local stiffness matrix and load vector on the elements e in the singular regions. Thus, the computer implementation of our method is quite simple since any existing finite element code can be used for the computation of the right-hand sides of (12)–(13) without any alterations. Furthermore, if $\mu = 0$ and $f = 0$ on S, our method does not require any extra work.

Suppose $e_1 \in \mathscr{T}_0$, $e_2 \in \mathscr{T}_S$, and $\gamma = e_1 \cap e_2 = \{(r_0, \theta) : a \leqslant \theta \leqslant b\}$. Then the conformal mapping $(\varphi^\omega)^{-1}$ is linear on the closed interval $[a, b]$ and hence the basis functions constructed by using the usual elemental mapping Φ_e for $e \subset \Omega_0$ and the singular elemental mapping Φ_e^S for $e \subset S$ are continuous along their common edges γ.

Thus far, for brevity, the method was explained for the case of one corner singularity. The argument is similar to the case when the problem contains many singularities of different types (we refer to [4] for the corner singularities, to [20] for the boundary data singularities, to [21] for interface singularities).

Suppose u_{ex} has corner singularities at $P_1, \ldots, P_M$. For each q, let S_q be the singular region determined by Step 1, $\omega_q \pi$ be the interior angle at P_q, φ^{ω_q} be the auxiliary mapping determined by Step 2, $\mathscr{T}_q$ be the triangulation on S_q determined by Step 3. Suppose $u_{\mathrm{ex}}|_{\Omega_0} \in H^{k_0}(\Omega_0)$ and $u_{\mathrm{ex}}|_{\Omega_q} \in H^{k_q}(\Omega_q)$, $1 \leqslant q \leqslant M$. Then without loss of generality we can assume that $(k_0 - 1) \geqslant 1$, $0 < (k_q - 1) < 1$, for each q, $1 \leqslant q \leqslant M$. Since ω_q was assumed to be > 1, $\hat{u}_{\mathrm{ex}} = u_{\mathrm{ex}}|_{\Omega_q} \circ \varphi^{\omega_q} \in H^{k_q^*}(\Omega_q^*)$ and $(k_q^* - 1) > 1$. Here $\varphi^{\omega_q}(\Omega_q^*) = \Omega_q$. The following results were proven in [4, 20].

THEOREM 2.1. (1) *Suppose $u_p^{(\omega_1, \ldots, \omega_M)}$ is the finite element solution obtained by employing the method of auxiliary mapping with the auxiliary mapping φ^{ω_q} on each singular region Ω_q in the framework of the p-version of the finite element method. Then we have*

$$\|u_p^{(\omega_1, \ldots, \omega_M)} - u_{\mathrm{ex}}\|_{1,\Omega} \leqslant \left[C_0 \frac{\|u_{\mathrm{ex}}\|_{k_0, \Omega_0}}{N_p^{(k_0 - 1)/2}} + \sum_{q=1}^{M} C_q \frac{\|\hat{u}_{\mathrm{ex}}\|_{k_q^*, \Omega_q^*}}{N_p^{(k_q^* - 1)/2}} \right], \quad (14)$$

where N_p is the degree of freedom and, for each q, $0 \leqslant q \leqslant M$, C_q is independent of N_p.

(2) *Let u_p^h be the finite element solution obtained by employing the method of auxiliary mapping with the auxiliary mapping $\varphi^{\omega_q} : z = \xi^{\omega_q}$ in the framework of the h-p version of the finite element method; then*

$$\|u_{\mathrm{ex}} - u_p^h\|_{1,\Omega} \leqslant \left[C_0 \frac{h^{\mu_0 - 1}}{p^{k_0 - 1}} \|u_{\mathrm{ex}}\|_{k_0, \Omega_0} + \sum_{q=1}^{2} C_j \frac{h^{\mu_q - 1}}{p^{k_q^* - 1}} \|\hat{u}_{\mathrm{ex}}\|_{k_q^*, \Omega_q^*} \right],$$

where $u_0 = \min(p + 1, k_0)$, $\mu_q = \min(p + 1, k_q^*)$, for $q = 1, \ldots, M$, and the constants C_q are independent of the polynomial degree p, the mapping size ω_q, and the length of the largest side h.

2.2. Chebyshev Collocation Method

In the most common Chebyshev collocation method, the collocation points in the interval $[-1, 1]$ are chosen to be the extrema

$$x_j = \cos \frac{\pi j}{N} \qquad (j = 0, \ldots, N) \quad (15)$$

of the Nth-order Chebyshev polynomials $T_N(x)$. Here the Chebyshev polynomial of degree n is defined by

$$T_n(x) = \cos(n \cos^{-1} x). \tag{16}$$

In order to construct the interpolant of $u(x)$ at the point x we define the polynomials

$$\phi_j(x) = \frac{(1-x^2)\, T_N'(x)(-1)^{j+1}}{\bar{c}_j N^2 (x - x_j)} \qquad (j = 0, ..., N) \tag{17}$$

with $\bar{c}_0 = \bar{c}_N = 2$, $\bar{c}_j = 1$ $(1 \leqslant j \leqslant N-1)$. It is readily verified that $\phi_j(x_k) = \delta_{jk}$.

The Nth-degree interpolation polynomial, $P_N u(x)$, to $u(x)$ is given by

$$P_N u(x) = \sum_{j=0}^{N} u(x_j)\, \phi_j(x). \tag{18}$$

Alternatively, $P_N u(x)$ can be expressed in terms of series expansion of Chebyshev polynomials,

$$P_N u(x) = \sum_{n=0}^{N} a_n T_n(x), \tag{19}$$

where

$$a_n = \frac{2}{N} \frac{1}{\bar{c}_n} \sum_{j=0}^{N} \frac{u(x_j)\, T_n(x_j)}{\bar{c}_j}. \tag{20}$$

It should be noted that the coefficients a_n in (20) can be evaluated by using the FFT. In fact, using (16) in (20) gives

$$a_n = \frac{2}{N} \frac{1}{\bar{c}_n} \sum_{j=0}^{N} \frac{u(x_j)}{\bar{c}_j} \cos \frac{\pi j n}{N}. \tag{21}$$

The second step in getting a collocation approximation is to express the derivatives of $P_N u$ in terms of $u(x)$ at the collocation points x_j. This can be done by differentiating either (18) or (19). With (19) we obtain

$$\frac{d^s}{dx^s} P_N u(x) = \sum_{j=0}^{N} u(x_j) \frac{d^s}{dx^s} \phi_j(x) \tag{22}$$

so that

$$\frac{d^s}{dx^s} P_N u(x_k) = \sum_{j=0}^{N} u(x_j) (D_N^s)_{k,j}, \tag{23}$$

where

$$(D_N^s)_{k,j} = \frac{d^s}{dx^s} \phi_j(x)|_{x = x_k}. \tag{24}$$

For example,

$$\begin{aligned} (D_N^1)_{k,j} &= \frac{\bar{c}_k (-1)^{j+k}}{\bar{c}_j x_k - x_j} \qquad (k \neq j), \\ (D_N^1)_{j,j} &= -\frac{x_j}{2(1-x_j^2)}, \\ (D_N^1)_{0,0} &= \frac{2N^2+1}{6} = -(D_N^1)_{N,N}, \end{aligned} \tag{25}$$

and

$$D_N^p = (D_N^1)^p. \tag{26}$$

2.2.A. *Chebyshev Collocation Method for the One-Dimensional Problem*

Let us consider

$$\begin{aligned} -U_{xx} &= f \qquad \text{in } (-1, 1), \\ U(x_0) &= g^+, \qquad U(x_N) = g^-, \end{aligned} \tag{27}$$

where $x_0 = 1$ and $x_N = -1$.

The collocation approximation of (27) results in the algebraic system of equations for the unknowns $u_j = u(x_j)$, $0 \leqslant j \leqslant N$,

$$\begin{aligned} -\sum_{j=0}^{N} u(x_j)(D_N^2)_{k,j} &= f(x_k), \qquad 1 \leqslant k \leqslant N-1, \\ u_0 &= g^+, \qquad u_N = g^-, \end{aligned} \tag{28}$$

where $u_0 = u(x_0)$ and $u_N = u(x_N)$. Let

$$\boldsymbol{\alpha}_N = ((D_N^2)_{1,0}, (D_N^2)_{2,0}, ..., (D_N^2)_{N-1,0})^{\mathrm{T}}, \tag{29}$$

$$\boldsymbol{\beta}_N = ((D_N^2)_{1,N}, (D_N^2)_{2,N}, ..., (D_N^2)_{N-1,N})^{\mathrm{T}}, \tag{30}$$

and

$$D_{N'}^2 = ((D_N^2)_{k,j}), \qquad 1 \leqslant k, j \leqslant N-1. \tag{31}$$

Then

$$D_N^2 = \begin{pmatrix} (D_N^2)_{0,0} & \cdots & (D_N^2)_{0,N} \\ \boldsymbol{\alpha}_N & D_{N'}^2 & \boldsymbol{\beta}_N \\ (D_N^2)_{N,0} & \cdots & (D_N^2)_{N,N} \end{pmatrix}. \tag{32}$$

Thus (28) becomes

$$-(\boldsymbol{\alpha}_N, D_{N'}^2, \boldsymbol{\beta}_N) \begin{pmatrix} u_0 \\ u_1 \\ \vdots \\ u_{N-1} \\ u_N \end{pmatrix} = \mathbf{f}, \tag{33}$$

where $\mathbf{f}=(f_0, ..., f_N)^T$, $u_j=u(x_j)$, $f_j=f(x_j)$. Since $u_0=g^+$ and $u_N=g^-$, from (32) we can obtain the algebraic equations

$$-D_{N'}^2\mathbf{u}=\mathbf{f}+g^+\boldsymbol{\alpha}_N+g^-\boldsymbol{\beta}_N, \tag{34}$$

where $\mathbf{u}=(u_1, u_2, ..., u_{N-1})^T$.

2.2.B. *Chebyshev Collocation Method for the Two-Dimensional Problem*

Let us consider the Helmholtz equation

$$\begin{aligned} -\Delta U+\mu U&=f \qquad \text{in } \Omega,\\ U&=g \qquad \text{on } \partial\Omega, \end{aligned} \tag{35}$$

where $\Omega=[-1, 1]\times[-1, 1]$. For a general rectangular domain $\Omega'=[-a, b]\times[-c, d]$, we can use the affine transformation that maps Ω into Ω'. Like the one-dimensional problem, we choose the following Chebyshev collocation nodes:

$$x_i=\cos\frac{\pi i}{N} \qquad (0\leqslant i\leqslant N), \tag{36}$$

$$y_j=\cos\frac{\pi j}{M} \qquad (0\leqslant j\leqslant M). \tag{37}$$

The two-dimensional Lagrange polynomials are defined by the tensor product of the one-dimensional counterparts in x- and y-spatial directions with appropriate degrees,

$$\begin{aligned} \Phi_{ij}(x, y)&=\frac{(-1)^{i+1}(1-x^2)\,T'_N(x)}{\bar{c}_i N^2(x-x_i)}\\ &\quad\times\frac{(-1)^{j+1}(1-y^2)\,T'_M(y)}{\bar{d}_j M^2(y-y_j)}\\ &=\phi_i^N(x)\,\phi_j^M(y), \end{aligned} \tag{38}$$

where $\bar{c}_0=\bar{c}_N=\bar{d}_0=\bar{d}_M=2$, $\bar{c}_i=1$ $(1\leqslant i\leqslant N-1)$, $\bar{d}_j=1$ $(1\leqslant j\leqslant M-1)$.

It is also readily verified that

$$\Phi_{ij}(x_l, y_m)=\delta_{il}\delta_{jm}. \tag{39}$$

The interpolant polynomial, $P_{NM}u(x, y)$, to $u(x, y)$ is given by

$$P_{NM}u(x, y)=\sum_{i=0}^{N}\sum_{j=0}^{M}u(x_i, y_j)\,\Phi_{ij}(x, y). \tag{40}$$

Let $u_{ij}=u(x_i, y_j)$; then with given Dirichlet boundary conditions we have only $(N-1)\times(M-1)$ unknowns u_{ij} $(1\leqslant i\leqslant N-1,\ 1\leqslant j\leqslant M-1)$. We put the unknowns $\{u_{ij}\}$ into vector form in two different ways,

$$\mathbf{U}=\begin{pmatrix}\mathbf{u}_1\\ \mathbf{u}_2\\ \vdots\\ \mathbf{u}_{M-1}\end{pmatrix}, \qquad \mathbf{V}=\begin{pmatrix}\mathbf{v}_1\\ \mathbf{v}_2\\ \vdots\\ \mathbf{v}_{N-1}\end{pmatrix},$$

where $\mathbf{u}_i=(u_{1,i}, u_{2,i}, ..., u_{N-1,i})^T$ and $\mathbf{v}_j=(u_{j,1}, u_{j,2}, ..., u_{j,M-1})^T$. Then, for fixed y_j,

$$D_{N'}^2\mathbf{u}_j+\boldsymbol{\alpha}_N g_j^+ +\boldsymbol{\beta}_N g_j^- \tag{41}$$

gives $\partial^2u/\partial x^2$ along the jth row mesh points, where $\boldsymbol{\alpha}_N$ and $\boldsymbol{\beta}_N$ are vectors defined in (29)–(30) and $g_j^+=g(x_0, y_j)$, $g_j^-=g(x_N, y_j)$, $1\leqslant j\leqslant M-1$. Therefore,

$$\begin{aligned} &\begin{pmatrix}D_{N'}^2 & & & \\ & D_{N'}^2 & & \\ & & \ddots & \\ & & & D_{N'}^2\end{pmatrix}\begin{pmatrix}\mathbf{u}_1\\ \mathbf{u}_2\\ \vdots\\ \mathbf{u}_{M-1}\end{pmatrix}\\ &\quad+\begin{pmatrix}g_1^+\boldsymbol{\alpha}_N\\ g_2^+\boldsymbol{\alpha}_N\\ \vdots\\ g_{M-1}^+\boldsymbol{\alpha}_N\end{pmatrix}+\begin{pmatrix}g_1^-\boldsymbol{\beta}_N\\ g_2^-\boldsymbol{\beta}_N\\ \vdots\\ g_{M-1}^-\boldsymbol{\beta}_N\end{pmatrix} \end{aligned} \tag{42}$$

is $\partial^2u/\partial x^2$ evaluated at all interior nodes, arranged in a row by row order.

Similarly,

$$\begin{aligned} &\begin{pmatrix}D_{M'}^2 & & & \\ & D_{M'}^2 & & \\ & & \ddots & \\ & & & D_{M'}^2\end{pmatrix}\begin{pmatrix}\mathbf{v}_1\\ \mathbf{v}_2\\ \vdots\\ \mathbf{v}_{M-1}\end{pmatrix}\\ &\quad+\begin{pmatrix}h_1^+\boldsymbol{\alpha}_M\\ h_2^+\boldsymbol{\alpha}_M\\ \vdots\\ h_{N-1}^+\boldsymbol{\alpha}_M\end{pmatrix}+\begin{pmatrix}h_1^-\boldsymbol{\beta}_M\\ h_2^-\boldsymbol{\beta}_M\\ \vdots\\ h_{N-1}^-\boldsymbol{\beta}_M\end{pmatrix} \end{aligned} \tag{43}$$

gives $\partial^2u/\partial y^2$ evaluated at all interior nodes, but arranged in a column by column order, where $h_i^+=g(x_i, y_0)$ and $h_i^-=g(x_i, y_M)$, $1\leqslant i\leqslant N-1$.

We know that for our vectors $\mathbf{U}$ and $\mathbf{V}$ there exists a permutation matrix P such that

$$\mathbf{U}=P\mathbf{V}. \tag{44}$$

Let us denote the $(N-1)\times(M-1)$ by $(N-1)\times(M-1)$ block matrices by

$$D_x=\begin{pmatrix} D_{N'}^2 & & & \\ & D_{N'}^2 & & \\ & & \ddots & \\ & & & D_{N'}^2 \end{pmatrix} \tag{45}$$

and

$$D_y=\begin{pmatrix} D_{M'}^2 & & & \\ & D_{M'}^2 & & \\ & & \ddots & \\ & & & D_{M'}^2 \end{pmatrix}, \tag{46}$$

and also let

$$\mathbf{F}=\begin{pmatrix} \mathbf{f}_1 \\ \mathbf{f}_2 \\ \vdots \\ \mathbf{f}_{M-1} \end{pmatrix}, \tag{47}$$

where $\mathbf{f}_i=(f_{1i}, f_{2i}, \ldots, f_{(N-1)i})^{\mathrm{T}}$, $1\leqslant i\leqslant M-1$.

Then, by combining (42) and (43) we have the following Chebyshev collocation approximation to (35):

$$\begin{aligned} -(D_x+PD_yP^{-1}-\mu I)\mathbf{U} &= \begin{pmatrix} g_1^+\boldsymbol{\alpha}_N \\ g_2^+\boldsymbol{\alpha}_N \\ \vdots \\ g_{M-1}^+\boldsymbol{\alpha}_N \end{pmatrix}+\begin{pmatrix} g_1^-\boldsymbol{\beta}_N \\ g_2^-\boldsymbol{\beta}_N \\ \vdots \\ g_{M-1}^-\boldsymbol{\beta}_N \end{pmatrix} \\ &\quad + P\begin{pmatrix} h_1^+\boldsymbol{\alpha}_M \\ h_2^+\boldsymbol{\alpha}_M \\ \vdots \\ h_{N-1}^+\boldsymbol{\alpha}_M \end{pmatrix}+P\begin{pmatrix} h_1^-\boldsymbol{\beta}_M \\ h_2^-\boldsymbol{\beta}_M \\ \vdots \\ h_{N-1}^-\boldsymbol{\beta}_M \end{pmatrix}+\mathbf{F}. \end{aligned} \tag{48}$$

2.3. The Iterative Method for the Helmholtz Equation

The high order basis functions in spectral methods disagree with the low order basis functions in the finite element method along the interfaces. Thus the coupling process will lead to discontinuous trial functions. We have investigated an iterative method to deal with this matching problem.

Let us describe the iterative method proposed in [11, 26]. Consider a simple rectangular domain $\Omega=[-1,1]\times[-a,b]$ with $a,b>0$, decomposed in the subsets $\Omega_1=[-1,1]\times[0,b]$, $\Omega_2=[-1,1]\times[-a,0]$. We denote by $\Gamma=[-1,1]\times\{0\}$ the interface between Ω_1 and Ω_2, and by $\partial\Omega$ the boundary of Ω. Then for all square-integrable functions f, g and nonnegative constant μ, we consider the following Helmholtz equation:

$$\begin{aligned} -\Delta u+\mu u &= f \quad \text{in } \Omega, \\ u &= g \quad \text{on } \partial\Omega, \end{aligned} \tag{49}$$

If v denotes the restriction of u to Ω_1 and w denotes the one to Ω_2, then (49) can be written in the split form,

$$\begin{aligned} -\Delta v+\mu v &= f \quad \text{in } \Omega_1, \\ v &= g \quad \text{on } \partial\Omega_1\backslash\Gamma, \\ v &= w \quad \text{on } \Gamma, \\ \frac{\partial w}{\partial n} &= \frac{\partial v}{\partial n} \quad \text{on } \Gamma, \end{aligned} \tag{50}$$

$$\begin{aligned} w &= g \quad \text{on } \partial\Omega_2\backslash\Gamma, \\ -\Delta w+\mu w &= f \quad \text{in } \Omega_2, \end{aligned} \tag{51}$$

where $\partial/\partial n$ denotes the normal derivative along interface Γ.

An analogous statement also holds for decompositions of the domain Ω into any finite number of disjoint subdomains. In such a case, continuity of the function and of its first derivative should be enforced at each interface boundary.

We introduce the following iterative procedure in order to solve (50)–(51). Let λ_1 be any given function on Γ. We consider the two sequences of functions $v^{(n)}$ and $w^{(n)}$, $n\geqslant 1$, which are the solutions of the two problems, respectively,

$$\begin{aligned} -\Delta v^{(n)}+a_0 v^{(n)} &= f \quad \text{in } \Omega_1, \\ v^{(n)} &= g \quad \text{on } \partial\Omega_1\backslash\Gamma, \\ v^{(n)} &= \lambda_n \quad \text{on } \Gamma, \end{aligned} \tag{52}$$

and

$$\begin{aligned} -\Delta w^{(n)}+a_0 w^{(n)} &= f \quad \text{in } \Omega_2, \\ w^{(n)} &= g \quad \text{on } \partial\Omega_2\backslash\Gamma, \\ \frac{\partial w^{(n)}}{\partial y} &= \frac{\partial v^{(n)}}{\partial y} \quad \text{on } \Gamma, \end{aligned} \tag{53}$$

where

$$\lambda_{n+1}=\theta w^{(n)}+(1-\theta)\lambda_n \quad \text{on } \Gamma, \quad n\geqslant 1, \tag{54}$$

and $\theta\in(0,1]$ is a relaxation parameter. The problems have the inherited boundary conditions along $\partial\Omega_1\backslash\Gamma$ and $\partial\Omega_2\backslash\Gamma$, respectively. If the sequences $\{v^{(n)}\}$ and $\{w^{(n)}\}$ converge, their limits are necessarily the solutions v and w to (50)–(51). Let

$$c(\theta)=\sup_{k\geqslant 1}|c_k(\theta)|. \tag{55}$$

where $c_k(\theta) = 1 - \theta(1 + \rho(k))$ for $k \geq 1$, $\rho(t) = \tanh(\sqrt{t}\, b)/\tanh(\sqrt{t}\, a)$, $t > 0$. Then, for the Helmholtz equation with homogeneous boundary condition (i.e., $g = 0$), it is proven in [11] that for all λ_1, a, and b, the iterative procedure (52)–(54) converges if and only if $c(\theta) < 1$.

3. NUMERICAL RESULTS

In this section, we give numerical results obtained by applying our method to Helmholtz equations with Dirichlet boundary conditions. We also compare the results obtained by our coupling method with those obtained by the finite element method.

First, we apply the coupling method to the Helmholtz equation by dividing the solution domain Ω into two subdomains; Ω is the L-shaped domain as depicted in Fig. 3.1. The case when the domain is divided into three subdomains is discussed in Test Two.

Test One. Let us consider the Helmholtz problem, (49), with $\mu = 1$ on the L-shaped domain as depicted in Fig. 3.1. Suppose $f = g = r^{2/3}\sin(2/3)\theta$. Then $u(r, \theta) = r^{2/3}\sin(2/3)\theta$ is the true solution of (49), with $\mu = 1$, and hence this problem is actually Laplace equation. Thus the results obtained by applying our method to the Helmholtz equation with nonhomogeneous Dirichlet boundary condition is expected to be the same as those obtained by applying our method to the Laplace equation. Hence, from Theorem 2.1, an exponential convergence is expected when the method of auxiliary mapping was used in the finite element part of the coupling method.

In order to apply our coupling method to the problem (49), the domain Ω is decomposed into a rectangular subdomain Ω_{sp}, on which the true solution u_{ex} is analytic and a nonrectangular subdomain Ω_{fe}, on which u_{ex} has a corner singularity. The subdomains Ω_{sp}, Ω_{fe}, and the mesh on Ω_{fe} for the finite element method are depicted in Fig. 3.1.

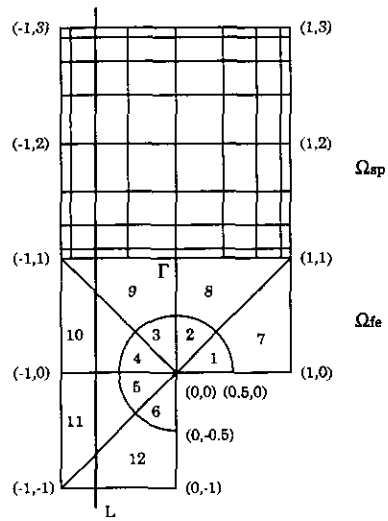

FIG. 3.1. The L-shaped domain with one singularity (re-entrant corner) and the line L.

TABLE I

$\mathrm{Err}_\infty(\Gamma)$ at Each Iteration until Convergence Is Achieved

	Without mapping			With mapping		
NIT	$N=4$ $p=2$	$N=8$ $p=4$	$N=16$ $p=8$	$N=4$ $p=2$	$N=8$ $p=4$	$N=16$ $p=8$
1	0.587D-00	0.963D-00	0.764D-00	0.995D-00	0.963D-00	0.964D-00
2	0.265D-00	1.610D-02	1.555D-02	2.292D-02	2.161D-02	1.727D-02
3	0.146D-00	3.492D-03	2.559D-04	1.377D-03	5.725D-04	2.911D-04
4	0.102D-00	7.754D-04	5.337D-05	9.480D-04	1.352D-04	5.252D-06
5	8.622D-02	6.341D-04	4.814D-05	9.127D-04	1.290D-04	8.031D-07
6	8.015D-02	6.217D-04	4.810D-05	Stop	Stop	3.421D-07
7	Stop	Stop	Stop			2.206D-07
8						1.816D-07
9						Stop

Note. Three mesh sizes are reported here.

Let $\Gamma = \Omega_{sp} \cap \Omega_{fe}$ be the common boundary of two subdomains. We choose λ_1 as a linear interpolation of $u_{ex}(1, 1)$ and $u_{ex}(-1, 1)$. Let $u_{sp}^{(1)}$ be the solution of

$$-\Delta u_{sp} + u_{sp} = f \qquad \text{in } \Omega_{sp}, \tag{56}$$

$$u_{sp} = g \qquad \text{on } \partial\Omega_{sp}\backslash\Gamma, \tag{57}$$

$$u_{sp} = \lambda_1 \qquad \text{on } \Gamma, \tag{58}$$

obtained by the spectral method. Now, let $u_{fe}^{(1)}$ be the solution of the mixed boundary value problem

$$-\Delta u_{fe} + u_{fe} = f \qquad \text{in } \Omega_{fe}, \tag{59}$$

$$u_{fe} = g \qquad \text{on } \partial\Omega_{fe}\backslash\Gamma, \tag{60}$$

$$\frac{\partial u_{fe}}{\partial n} = \frac{\partial u_{sp}^{(1)}}{\partial n} \qquad \text{on } \Gamma, \tag{61}$$

obtained by the p-version of the finite element method. Then the Dirichlet boundary condition along Γ for the second iteration is determined as follows:

$$\lambda_2 = \theta u_{fe}^{(1)} + (1 - \theta)\,\lambda_1.$$

TABLE II

The Error in Maximum Norm on Ω_{sp}^* and Ω_{fe}

		Without Mapping			With Mapping		
N	p-deg	$\mathrm{Err}_\infty(\Omega_{sp}^*)$	$\mathrm{Err}_\infty(\Omega_{fe})$	NIT	$\mathrm{Err}_\infty(\Omega_{sp}^*)$	$\mathrm{Err}_\infty(\Omega_{fe})$	NIT
4	2	3.374D-02	2.759D-02	6	1.342D-04	1.248D-04	5
8	4	4.009D-05	3.755D-04	6	1.178D-04	9.593D-05	5
16	8	7.123D-06	1.401D-04	6	3.574D-10	6.154D-07	6

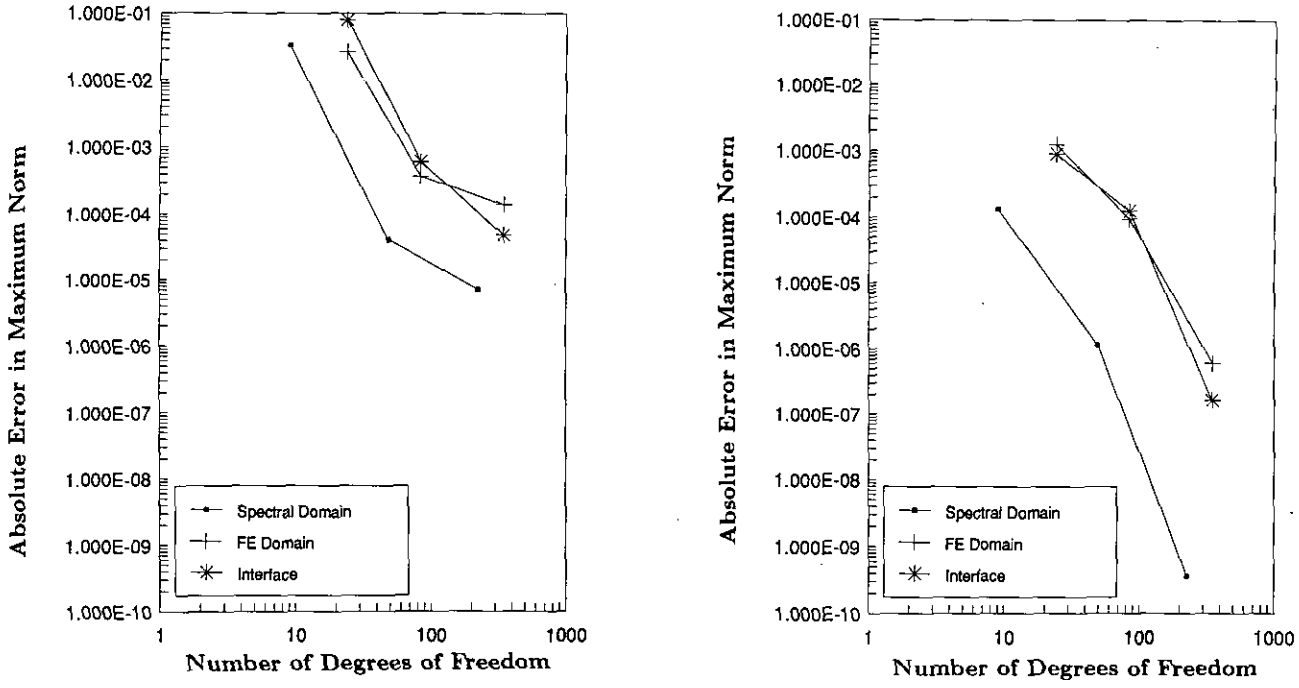

FIG. 3.2. The convergence history on various regions of the L-shaped domain with one singularity when (a) no mapping technique is used. (b) the mapping technique is used.

This iterative process can be repeated until the desired convergence is obtained. The optimal choice of the relaxation parameter θ should be chosen dynamically for each iteration. However, in our computations, the relaxation parameter θ is chosen to be 0.51 at each iteration step and a satisfactory rate of convergence is observed.

Throughout this section, $\mathrm{Err}_\infty(E)$, NIT, N, p, and DOF denote *the absolute error in the maximum norm on the domain E, the number of iterations, the polynomial degree in each variable of the spectral solution in* Ω_{sp}, *the polynomial degree of the basis functions for finite element solution in* Ω_{fe}, and *the number of degrees of freedom*, respectively.

The errors in maximum norm for finite element solutions are computed by evaluating the absolute error at 25 points per element and those for the spectral solutions are calculated by evaluating errors at collocation points. Henceforth, we assume $p \leqslant 8$.

It is observed that the maximum error occurs along the

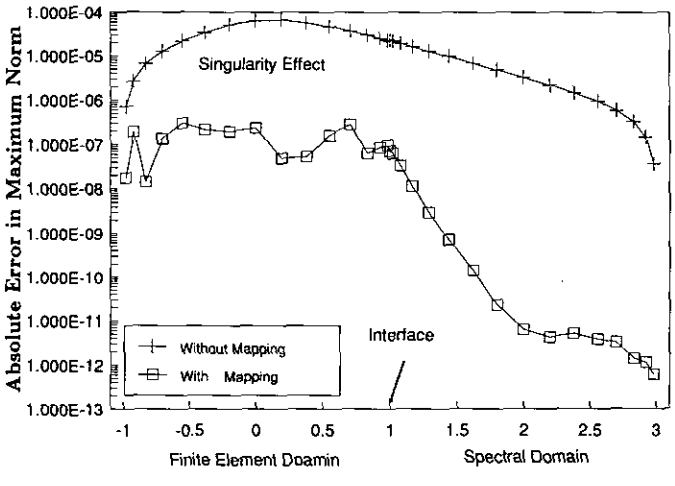

FIG. 3.3. The profiles of absolute errors along the line L, depicted in Fig. 3.1.

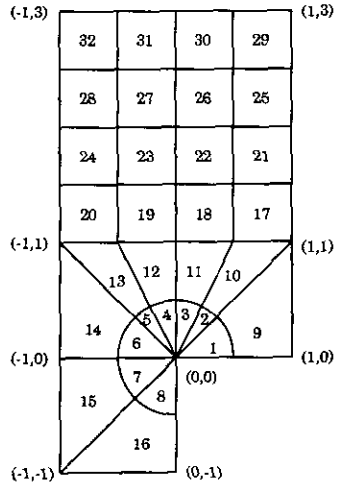

FIG. 3.4. The L-shaped domain with one singularity (re-entrant corner) and mesh on this domain for the full finite element algorithm.

TABLE III

The Maximum Errors of Finite Element Solutions

(a) *Using the mapping technique*

p-deg	$\mathrm{Err}_\infty(\Omega_1)$	$\mathrm{Err}_\infty(\Omega_2)$	$\mathrm{Err}_\infty(\Omega_3)$	$\mathrm{Err}_\infty(\Omega_4)$	$\mathrm{Err}_\infty(\Omega_5)$
2	4.02D-02	4.37D-03	1.31D-03	6.01D-04	1.91D-04
4	2.97D-03	8.89D-04	2.77D-04	1.00D-04	3.67D-05
6	1.01D-03	3.34D-04	9.83D-05	3.71D-05	1.43D-05
7	1.66D-03	2.36D-04	6.76D-05	2.55D-05	9.75D-06
8	1.53D-03	1.57D-04	4.82D-05	1.82D-05	6.99D-06

(b) *Using the mapping technique*

2	1.69D-03	2.54D-03	4.01D-04	1.71D-04	6.61D-05
4	1.72D-04	2.15D-04	5.07D-05	1.08D-05	2.32D-06
6	1.13D-05	1.13D-04	1.87D-06	2.25D-07	3.34D-08
7	2.47D-06	2.47D-06	3.36D-07	2.19D-08	3.30D-09
8	5.27D-07	5.27D-07	6.68D-08	2.70D-09	6.35D-10

interface Γ. Because of the lower order accuracy on Ω_{fe} (large elements are used as shown in Fig. 3.1), we select a subregion, $\Omega_{\mathrm{sp}}^* = \{(x, y) \in \Omega_{\mathrm{sp}} : y \geqslant 1.5\}$, of the domain Ω_{sp}, where the influence from the interface will be smaller and high order accuracy of spectral methods can be expected.

In all of our numerical experiments, the error on the interface $\mathrm{Err}_\infty(\Gamma)$ for each iteration decays very rapidly; then it fluctuates around some equilibrium values. The general convergent history is not sensitive to the initial choice of λ_1, which is a promising indication of the effectiveness of the coupling methods. We stop the iteration process when the change in $\mathrm{Err}_\infty(\Gamma)$ is $\leqslant 10\%$.

In Table I we report the convergence history of $\mathrm{Err}_\infty(\Gamma)$ along the interface Γ for both cases: when the method of auxiliary mapping is not used and when it is used (for a finite element solution). In Table II, we show the maximum errors on Ω_{sp}^* and Ω_{fe} for the results at the last iterations. In Fig. 3.2, we plot the maximum errors on three parts (that is, Ω^*, Γ, Ω_{fe}) of the solution domain for three different sizes of meshes for the coupling methods. Fig. 3.2a corresponds to the case when no auxiliary mapping technique is used with the finite element method while Fig. 3.2b corresponds to the case where the mapping technique is used. By comparing Figs. 3.2a and b, one can see that the mapping technique leads to a dramatic improvement in accuracy. That is, one can see an exponential convergence in the latter case.

To see the profile of the change of error, in Fig. 3.3, we plot the maximum error in logarithmic scale of the solutions along a line L, depicted in Fig. 3.1, across the domain Ω. Once again, one can see the improvement by the mapping technique which can remove the pollution effect caused by the singularity.

In the tables in this paper, the columns labeled *without mapping* stand for the case when the method of auxiliary mapping is not applied for the finite element solution of our coupling method. On the other hand, the columns labeled *with mapping* stand for the case when the mapping technique is applied.

In order to compare the coupling method with the p-version of the finite element method, we apply the p-version of the finite element method to the same problem on the whole domain Ω with mesh depicted in Fig. 3.4.

TABLE IVa

The CPU Time for the Coupling Method

Spectral part				Finite element part					
N	CPU-Ab	CPU-LU	CPU-BF	p	CPU-Ab	CPU-LU	CPU-BF	NIT	CPU total
4				2	15.88	5.69	0.01	5	21.62
8	0.2	0.13	0.01	4	32.41	6.02	0.02	6	38.94
16	1.32	12.47	0.16	8	98.69	9.53	0.15	8	124.49

Note. The mapping technique is used on the finite element part.

TABLE IVb

The CPU Time for the p-Version of the Finite Element Method

	$p=1$	$p=2$	$p=3$	$p=4$	$p=5$	$p=6$	$p=7$	$p=8$
CPU-Ab	15.96	29.41	47.04	75.36	112.79	169.74	250.13	354.99
CPU-LU	10.13	10.55	10.53	11.21	12.49	14.92	18.61	29.92
CPU-BF	0.01	0.02	0.04	0.08	0.15	0.24	0.39	0.61
CPU-total	26.10	39.98	57.61	86.65	125.43	184.90	269.13	385.52

Note. The mapping techniques is used

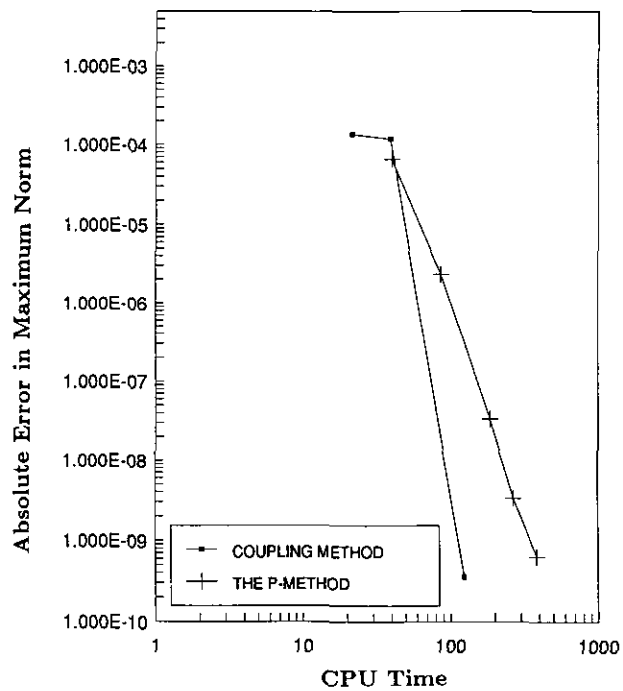

FIG. 3.5. Comparison of the coupling method and the p-version of the finite element method.

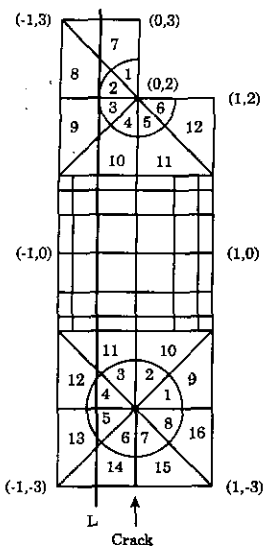

FIG. 3.6. The L-shaped domain with two singularities: A re-entrant corner and a crack.

Let $\Omega_1 = \bigcup_{1 \leqslant i \leqslant 8} e_i$, $\Omega_2 = \bigcup_{9 \leqslant i \leqslant 16} e_i$, $\Omega_3 = \bigcup_{17 \leqslant i \leqslant 20} e_i$, $\Omega_4 = \bigcup_{21 \leqslant i \leqslant 24} e_i$, $\Omega_5 = \bigcup_{25 \leqslant i \leqslant 32} e_i$, where e_i stands for the ith element (see Fig. 3.4). Then the maximum error in each subdomain is given by Tables III: Table IIIa is the case when the method of auxiliary mapping is not used and Table IIIb is the case when the mapping is used.

From Table IIIb, one can see that the maximum error is gradually decreasing from the region Ω_1 to the Ω_5. However, Table II shows that the coupling method yields high order accuracy throughout the subregion $\Omega_{sp}^* = \Omega_3 \cup \Omega_4 \cup \Omega_5$.

Next we present the CPU time comparison between the coupling method and the full p-version finite element methods (Tables IVa, IVb.) The final solution of the coupling method or the finite element method amounts to solving a system in the form $A\mathbf{x} = \mathbf{b}$. Thus, we use the following notations to denote the CPU time needed to complete different stages of solving this system: Let CPU-Ab, CPU-LU, CPU-BF, CPU-total stand for the CPU time required to generate the matrix A and load vector $\mathbf{b}$, calculate the factorization LU of the matrix A once, solve $LU\,\mathbf{x} = \mathbf{b}$ with backward and forward substitutions per iteration, and the total CPU time (all iterations are counted!), respectively. The load vector $\mathbf{b}$ should be calculated at each iteration. However, the factorization LU is done only once. Thus, the extra cost at each iteration is calculating $\mathbf{b}$ and solving $LU\,\mathbf{x}_{(n)} = \mathbf{b}$ with backward and forward substitutions.

$\mathrm{Err}_\infty(\Omega_5)$ in Table Vb and $\mathrm{Err}_\infty(\Omega_{sp}^*)$ in Table II versus CPU time is plotted in Fig. 3.5 (Note: $\Omega_5 \subset \Omega_{sp}^*$). One can conclude from Fig. 3.5 that our coupling method is cheaper than the finite element method when the spectral domain is larger than the finite element domain. In Table IVa, CPU time when $N = 4$ for the spectral part is too small to record.

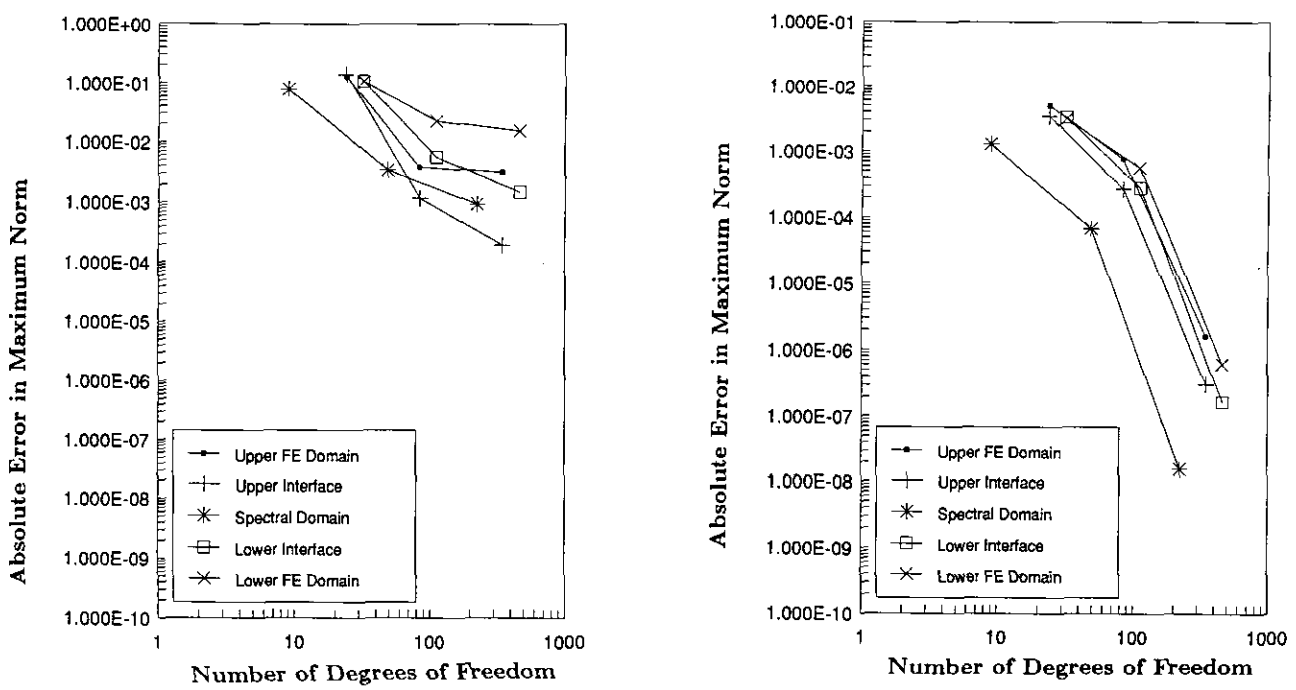

FIG. 3.7. The convergence history on various regions of the L-shaped domain with two singularities when (a) no mapping technique is used; (b) the mapping technique is used.

TABLE V

Each Iteration until Convergence Is Achieved[a]

	Without mapping			With mapping		
NIT	$N=4$ $p=2$	$N=8$ $p=4$	$N=16$ $p=8$	$N=4$ $p=2$	$N=8$ $p=4$	$N=16$ $p=8$
(a) $\mathrm{Err}_\infty(\Gamma_1)$						
1	1.721D-00	1.732D-00	1.744D-00	1.721D-00	1.740D-00	1.748D-00
2	2.633D-01	1.042D-01	1.078D-01	1.212D-01	8.203D-02	7.955D-03
3	1.300D-01	2.193D-03	5.962D-03	8.234D-03	2.338D-03	2.418D-03
4	1.107D-01	4.997D-03	9.964D-04	2.643D-03	2.271D-04	1.162D-04
5	1.070D-01	5.523D-03	1.456D-03	3.236D-03	2.745D-04	3.455D-06
6	Stop	Stop	Stop	Stop	Stop	4.191D-07
7						2.097D-07
8						1.644D-07
9						Stop
(b) $\mathrm{Err}_\infty(\Gamma_2)$[b]						
1	1.786D-00	1.701D-00	1.705D-00	1.786D-00	1.702D-00	1.705D-00
2	3.737D-00	1.265D-01	1.278D-01	1.045D-01	5.803D-02	5.835D-02
3	1.544D-01	7.467D-03	8.107D-03	6.178D-03	2.408D-03	2.480D-03
4	1.331D-01	5.294D-03	3.655D-04	1.621D-03	2.893D-04	7.685D-05
5	1.401D-01	1.117D-03	1.562D-04	2.958D-03	2.552D-04	3.882D-06
6	Stop	Stop	Stop	Stop	Stop	5.267D-07
7						3.790D-07
8						3.272D-07
9						Stop

[a] Three mesh sizes are reported.

[b] When the method of auxiliary mapping is and is not applied on Ω_{fe}^2.

As long as the interface Γ and the selection of the neighborhood S of the singularity (see Step 1 of the method of auxiliary mapping) do not make any "bad elements" on the finite element part, one can place the interface close to the neighborhood S in order to have the best results for a fixed number of DOF.

In the second test, we consider the case when the given domain Ω is decomposed into three subdomains.

Test Two. Let us consider the problem (49) on a domain Ω which contains two singularities (a re-entrant corner and a crack) as depicted in Fig. 3.6. Since the numerical results for $\mu = 1$ are similar to those for $\mu = 0$, we report the results obtained by applying the coupling method to the Poisson equation: $-\Delta u = f$ in Ω, $u = g$ on $\partial\Omega$. Suppose $g = u_1 \cdot u_2$ and $f = -\Delta(u_1 \cdot u_2)$, where

$$T_1(x, y) = (-(y+2), x),$$
$$w_1(r, \theta) = r^{1/2} \sin(\theta/2),$$
$$u_1(x, y) = w_1(T_1(x, y)),$$
$$T_2(x, y) = ((y-2), -x),$$
$$w_2(r, \theta) = r^{2/3} \sin(2\theta/3),$$
$$u_2(x, y) = w_2(T_2(x, y)).$$

Then $u_{\mathrm{ex}} = u_1 \cdot u_2$ is the true solution of the Poisson equation. Let

$$\Omega_{\mathrm{fe}}^1 = \{(x, y) \in \Omega : y \leqslant -1\},$$
$$\Omega_{\mathrm{fe}}^2 = \{(x, y) \in \Omega : 1 \leqslant y\},$$
$$\Omega_{\mathrm{sp}} = \{(x, y) \in \Omega : -1 \leqslant y \leqslant 1\},$$
$$\Omega_{\mathrm{sp}}^* = \{(x, y) \in \Omega : -0.5 \leqslant y \leqslant 0.5\}$$

and let $\Gamma_1 = \Omega_{\mathrm{fe}}^1 \cap \Omega_{\mathrm{sp}}$, $\Gamma_2 = \Omega_{\mathrm{fe}}^2 \cap \Omega_{\mathrm{sp}}$.

The convergence history of the maximum errors on both interface Γ_1 and Γ_2 are listed in Tables Va and b, respectively. As before, the iterations were stopped when the changes in both $\mathrm{Err}_\infty(\Gamma_1)$ and $\mathrm{Err}_\infty(\Gamma_2)$ are $< 10\%$. This rule is applied on Tables IIIa and b. Table VI shows the maximum errors on Ω_{sp}^*, Ω_{fe}^1, Ω_{fe}^2.

In Fig. 3.7, we plot the errors on various parts (that is, Ω_{fe}^1, Γ_1, Ω_{sp}^*, Γ_2, Ω_{fe}^2) of the solution domain for three different sizes of meshes for the coupling methods. Fig. 3.7a corresponds to the case when no auxiliary mapping technique is used with the finite element method while Fig. 3.7b

TABLE VI

The Error in Maximum Norm on Ω_{sp}^*, Ω_{fe}^1, and Ω_{fe}^2

N	p-deg	$\mathrm{Err}_\infty(\Omega_{\mathrm{sp}}^*)$	$\mathrm{Err}_\infty(\Omega_{\mathrm{fe}}^1)$	$\mathrm{Err}_\infty(\Omega_{\mathrm{fe}}^2)$	NIT
			Without mapping		
4	2	7.964D-02	1.070D-01	1.401D-01	5
8	4	3.442D-03	2.241D-02	3.759D-03	5
16	8	9.598D-04	1.542D-02	3.132D-03	8
			With mapping		
4	2	1.678D-03	3.236D-03	5.286D-03	5
8	4	6.881D-05	5.707D-04	7.687D-04	5
16	8	1.556D-08	5.408D-07	1.605D-06	8

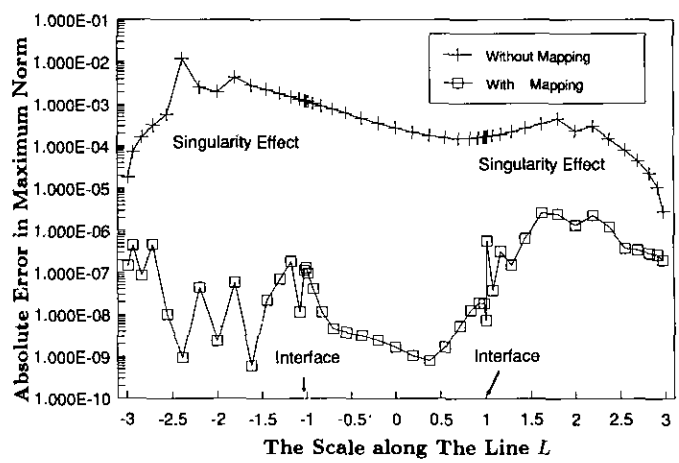

FIG. 3.8. The profiles of absolute errors along the line L, depicted in Fig. 3.6.

has the case where the mapping technique is used. Again in Fig. 3.8, we plot the maximum error in logarithmic scale of the solutions along a line L, depicted in Fig. 3.6. Across the domain Ω, we can see the improvement with the mapping technique in removing the singularity effects.

4. CONCLUSION

In our first attempt to couple spectral methods and the p-version of the finite element method, we obtained several promising results. In the numerical tests, we achieved the advantages of both methods: efficient handling of singularities caused by the irregular domain geometry and high accuracy of spectral methods by eliminating the pollution effects. We intend to extend our method to general elliptic equations as well as three-dimensional cases.

ACKNOWLEDGMENTS

The authors would like to thank Professor G. Karniadakis for valuable discussion during this work; thanks also are due to Professor D. Funaro for his suggestions.

REFERENCES

1. R. A. Adams, *Sobolev Spaces* (Academic Press, New York/London, 1975).
2. I. Babuška and B. Guo, *SIAM J. Math. Anal.* **19**, 172 (1988).
3. I. Babuška and B. Guo, *SIAM J. Numer. Anal.* **25**, 837 (1988).
4. I. Babuška and H. S. Oh, "The p-Version of the Finite Element Method for Domains with Corners and for Infinite Domains," *Numer. Methods Partial Diff. Eqs.* **6**, 371 (1990).
5. I. Babuška and M. Suri, *SIAM J. Numer. Anal.* **24**, 750 (1987).
6. I. Babuška and M. Suri, *Math. Modelling Numer. Anal.* **21**, 199 (1987).
7. I. Babuška, B. Szabo, and I. N. Katz, *SIAM J. Numer. Anal.* **18**, 515 (1981).
8. C. Bernardi, N. Debit, and Y. Maday, *Math. Comput.* **54**, 21 (1990).
9. W. Cai and C. W. Shu, *J. Comput. Phys.* (1991).
10. C. Canuto, M. Y. Hussaini, A. Quarteroni, and T. A. Zang, *Spectral Methods in Fluid Dynamics* (Springer-Verlag, Berlin/New York, 1988).
11. D. Funaro, A. Quarteroni, and P. Zanolli, *SIAM J. Numer. Anal.* **25**, 1213 (1988).
12. F. Gastaldi and A. Quarteroni, *Appl. Numer. Math.* **6**, 3 (1989).
13. F. Gastaldi, A. Quarteroni, and G. Sacchi Landriani, in *Third International Symposium on Domain Decomposition Methods for Partial Differential Equations* (SIAM, Philadelphia, PA, 1990), p. 22.
14. F. Gastaldi, A. Quarteroni, and G. Sacchi Landriani, *Comput. Methods Appl. Mech. Eng.* **80**, 347 (1989).
15. D. Gottlieb and S. A. Orszag, *Numerical Analysis of Spectral Methods: Theory and Applications* (SIAM-CBMS, Philadelphia, 1977).
16. P. Grisvard, *Elliptic Problems in Nonsmooth Domains*, Pitman, New York, 1985.
17. R. D. Henderson and G. E. Karniadakis, *Proceedings Unstructured Scientific Computations on Scalable Multi-Processors, ICASE, 1990* (MIT Press, Cambridge, MA, to appear).
18. V. A. Kontrat'ev, *Trans. Moscow Math. Soc.* **16**, 227 (1967).
19. K. Z. Korczak and A. T. Patera, "An isoparametric Spectral Element Method and its Application to Incompressible Two-Dimensional Flow in Complex Geometries," Proceedings, 6th GAMM Conference on Numerical Methods in Fluid Mechanics, Vieweg, 1986.
20. T. R. Lucas and H. S. Oh, The method of auxiliary mapping for the finite element solutions of elliptic problems containing singularities, *J. Comput. Phys.* **108**, 327 (1993).
21. H. S. Oh, and I. Babuška, *Comput. Methods Appl. Mech. Eng.* **97**, 211 (1992).
22. A. T. Patera, *J. Comput. Phys.* **54**, 173 (1984).
23. L. R. Scott, and M. Vogelius, *Mod. Math. Anal. Numer.* **19**, 111 (1985).
24. B. Szabó and I. Babuška, *Finite Element Analysis* (Wiley, New York, 1991).
25. E. Tadmor, *SIAM J. Numer. Anal.* **26**, 30 (1989).
26. P. Zanolli, *Calcolo*, to appear.